Asian Journal of Science and Applied Technology
ISSN: 2249-0698 (P)
Vol.13 No.2, 2024, pp.34-39

www.crijournals.org
DOI: https://doi.org/10.70112/ajsat-2024.13.2.4251

Hydrothermal Synthesis of Indium Oxide (In_2O_3) Semiconductor Photocatalyst Fabricated with Nitrogen-Sulfur Co-Doped Reduced Graphene Oxide (N,S-rGO)

Saidu Rabiu Saidu*, Zayyanu Iyya, Najib Muhammad, Bilyaminu Abdullahi, Momoh Shaibu and Rabiu Danhalilu
Department of Science Laboratory Technology, Federal Polytechnic Kaura Namoda, Zamfara, Nigeria
*Corresponding author: saidurabiusaidu@gmail.com
(Received 15 September 2024; Revised 2 October 2024; Accepted 6 November 2024; Available online 10 November 2024)

Abstract - **The main objective of this research project is to develop an efficient material for degrading pollutants from the textile and pharmaceutical industries, which seriously harm the environment and are challenging to remove from water bodies. This study aims to synthesize In_2O_3 and enhance its fundamental properties by fabricating it with a nitrogen and sulfur-reduced graphene oxide (N,S-rGO) heterostructure. Nanosized In_2O_3 was synthesized via a hydrothermal system and co-doped with N,S-rGO through a facile in-situ co-precipitation technique. The prepared samples were subjected to various characterization methods. XRD evaluation revealed that bare In_2O_3 has a rod-like structure with high crystallinity, while no characteristic diffraction peaks were observed for N,S-rGO and In_2O_3/N,S-rGO. FE-SEM and HR-TEM micrographs showed that In_2O_3 formed nanorods, N,S-rGO exhibited a thin-film layered structure, and In_2O_3/N,S-rGO presented a nanorod-layered structure. The nanorods had an average length of 200-500 nm, with particle sizes ranging from 1-4 µm. FT-IR spectra showed absorption peaks corresponding to In-O asymmetric vibrations and the in-plane deformation vibration of the O-H bond. Additionally, distinct vibrations corresponding to C=N, C-N, and C-S were noted. A strong and broad absorption peak was observed in the UV-VIS DRS evaluation, with a visible absorption edge at 460 nm for the photocatalysts. Bandgap studies revealed a moderate reduction in bandgap from the bare to the binary photocatalyst, with the ternary composite showing the lowest bandgap of 2.72 eV. The characterization results suggest that our In_2O_3/N,S-rGO nanocomposite is a feasible semiconductor photocatalyst that is inexpensive, easy to assemble, environmentally friendly, and effective at addressing recycling challenges, charge recombination, surface area, and bandgap issues.**

Keywords: **Photocatalyst, In_2O_3/N,S-rGO Nanocomposite, Bandgap, Pollutant Degradation, Hydrothermal Synthesis**

I. INTRODUCTION

The world's heavy reliance on fossil fuels, rapid industrial expansion, significant waste generation, and the increasing population are posing serious environmental challenges, resulting in a shortage of clean drinking water [1], [2]. The use of semiconductor materials and light energy in photocatalysis is a promising technique for environmental cleanup. Reactive oxygen species, including superoxide radicals, hydroxyl radicals, and hydrogen peroxide, are generated by excited electrons in a semiconductor photocatalyst, which then react with oxygen and water [3]. However, these electrons do not effectively contribute to the process; instead, they recombine with holes, releasing energy and reducing the quantum yield of photochemical reactions [4], [5].

The synthesis of nanoscale materials has garnered significant interest over the past 20 years. Metal oxide semiconductors are among the most attractive material types for functional nanomaterials. A substantial amount of research has focused on synthesizing catalyst-supported nanomaterials using techniques that are not substrate-specific but are compatible with various synthetic and fabrication methods. For instance, [6] synthesizes materials at the nanoscale, particularly metal oxide semiconductors, through catalyst-supported techniques that are compatible with diverse production strategies. In_2O_3, also known as amphoteric indium oxide, forms cubic crystals of the bixbyite type and is an example of a metal oxide. It is an n-type semiconductor with a body-centered cubic structure and a lattice parameter of a = 10.12 Å [7]. Initially reported with a bandgap of approximately 3.7 eV, it has been revised to around 2.9 eV [8]. Significant applications of In_2O_3-based photocatalysts include drug delivery in medical research, antimicrobial activity [9], and self-cleaning applications [10]. The work in [11] emphasizes the need for controlled synthesis of In_2O_3 materials with precise morphologies, such as nanowires, nanobelts, nanoparticles, nanotowers, microarrows, nanotubes, and lotus-root-like In_2O_3 nanorods. These morphologies significantly influence the performance of nanostructured materials [12], and are affected by factors like temperature, carrier gas flow, and substrate type [9]. Due to its relatively wide bandgap, In_2O_3 can absorb only a limited amount of radiation in the UV region of the solar spectrum, despite having excellent photocatalytic properties [13]. Wider bandgaps may lead to rapid recombination of photogenerated carriers, thus reducing photoactivity [14]. The common approach to address this issue is to engineer and shift the bandgap to the visible light region. However, metal oxides may produce recombination centers, which decrease photocatalytic activity, yet they also facilitate beneficial bandgap modifications.

Using non-metals as quantum dots is an efficient approach to reducing the bandgap of In_2O_3 [15]. Research has shown that doping In_2O_3 with non-metals such as C, N, and S creates oxygen vacancy defects [16], which can serve as charge-trapping sites and accelerate charge carrier separation. Among the various N-doping configurations, carbon atoms adjacent to pyridinic-N were found to be the most active sites. Increasing levels of sulfur have attracted considerable attention for sulfur-doped In_2O_3, as they can reduce the bandgap [17] and exhibit strong visible light absorption [18]. Photocatalytic activity is enhanced by dual doping with nitrogen and sulfur (N,S), which introduces structural defects in the carbon framework, improving electron delocalization and hole separation efficiency [19].

F. Wan, *et al.,* [20] produced a dual-defective ternary photocatalyst, ZnS/ZnO-In_2O_3, with large heterojunction interfaces and a porous layered structure, using an in situ etching growth approach and heat treatment. The study found that visible light photocatalysis performance improves when dual defects on ZnO and ZnS work in tandem to separate photogenerated charges. F. Gao, *et al.,* [21], studied that In_2D/3D In_2O_3/graphitic carbon nitride (g-C_3N_4) heterojunction (In_2O_3/OGCN) doped with oxygen was synthesized. Compared to pure In_2O_3 and OGCN, the enhanced In_2O_3/OGCN heterojunction demonstrated significant photocatalytic degradation capability, with results reported in the paper. This photocatalyst exhibited excellent physical stability and was recyclable.

A. Uddin, *et al.,* [22] successfully synthesized well-defined, flower-like In_2O_3 microrods through a one-step hydrothermal procedure followed by calcination. They achieved significant control over the morphology of the synthesized In_2O_3 samples. In the presence of glucose and urea, the data suggest that the template's synergistic effect contributes to the formation of flower-like In_2O_3 microrods.

Reduced graphene oxide (rGO) provides a promising alternative for photocatalysis, with double heteroatoms enhancing its activity. To increase the photoactivity of rGO, various semiconductors have been integrated with it [5]. Studies have shown that doping semiconductor photocatalysts with rGO can enhance their activity by reducing the recombination of photogenerated electron-hole pairs. Reduced graphene oxide is a single layer of two-dimensional (2D) carbon with sp^2 hybridization. It has a high surface area (2630 $m^2\ g^{-1}$), optical transparency, and chemical stability. However, consistently coating metal oxide nanoparticles with a carbon layer remains challenging. These factors make it critical to address the difficulty of creating ultrafine metal oxide nanoparticles with co-doped carbon layers.

To improve photocatalytic activity, it is essential to balance surface area and ease of photocatalyst recovery. While assembling N,S-codoped carbon-coated In_2O_3 nanoparticles may facilitate recycling, this often compromises surface area, reactive sites, and activity [23]. Achieving an optimal balance between surface area effects and photocatalyst recovery is essential for improving photocatalytic performance. Given its high electrocatalytic activity, N,S-rGO serves effectively as a cocatalyst in photocatalytic processes. The redistributed surface charge and electrostatic potential of graphene specifically make N,S-rGO/In_2O_3 more effective than other dual heteroatom-doped carbon materials for hydrogen evolution and permonosulfate activation. Consequently, the addition of N,S-codoped rGO nanoparticles to the In_2O_3 superstructure is expected to significantly enhance photocatalytic activity and potentially enable photocatalyst recovery.

II. METHODOLOGY

A. Synthesis of In_2O_3 Nanorods

The hydrothermal process was used to prepare In_2O_3 as reported in [16]. Typically, the synthesis involves dissolving 2 mmol of $InCl_3$ in 30 mL of deionized water, adding 3.5 g of glucose and 3.5 g of urea, and vigorously stirring the mixture for 1 h. The combined mixture was then transferred into a 50 mL Teflon-lined stainless-steel autoclave and maintained at 180 °C for 8 h. After allowing the autoclaved mixture to cool naturally to room temperature, a black precipitate was formed. The resulting deposits were separated by centrifugation and rinsed three times with ethanol and water. The material was then heated to 500 °C for 2 h in a tube furnace at a heating rate of 2 °C/min in a nitrogen environment, producing In_2O_3 microrods after a 12-h drying period at 80 °C in a vacuum oven.

B. Synthesis of Graphene Oxide (GO)

An adapted version of the Hummers' process was used to prepare GO [24]. Graphite powder (2 g) and $NaNO_3$ (1.5 g) were added to a flask, followed by the gradual addition of 46 mL of concentrated H_2SO_4 while stirring in an ice-water bath. Next, 7 g of $KMnO_4$ powder was gradually added with stirring, and the mixture was heated to 35 °C for 2 h. After heating to 90 °C for 30 min, 200 mL of deionized water was gradually added. Finally, 30 mL of H_2O_2 (5 wt%) was added as the temperature was allowed to drop to 60 °C.

C. Synthesis of Reduced Graphene Oxide (rGO)

After centrifuging the mixture and washing it with 100 mL of HCl solution (5 wt%) and 900 mL of deionized water, 1 g of graphite oxide was dispersed in 1,000 mL of deionized water using ultrasonication for 30 min. The mixture was then centrifuged at 1,000 rpm for 10 min, after which the solid was discarded, and the ultrasonic step was repeated three times. rGO was then isolated by centrifugation at 15,000 rpm for 30 min and dried at room temperature for 72 h.

D. Synthesis of N,S-rGO Nanosheet

To prepare N,S-rGO nanosheets, 1.2 g of thiourea was dispersed in 70 mL of deionized water using sonication for

15 min. Then, 70 mg of graphene oxide was added to the mixture and sonicated for 1 h. The resulting solution was transferred to a 100 mL Teflon-lined autoclave and heated at 180 °C for 12 h. The residue was washed with deionized water and ethanol, then dried at 70 °C for 12 h.

E. Synthesis of In_2O_3/N,S-rGO Nanocomposite

The ternary nanocomposite was prepared using an in-situ co-precipitation method. A homogeneous solution was produced by ultrasonically dispersing 0.40 g of In_2O_3 in 40 mL of deionized water, followed by dissolving 40 mg of N,S-rGO in 20 mL of deionized water and adding it to the above suspension. The two suspensions were vigorously stirred for 4 h, after which the sediments were collected by vacuum filtration and washed repeatedly with ultrapure water and ethanol. Finally, the In_2O_3/N,S-rGO samples were heated at a rate of 3 °C/min for 2 h at 250 °C.

III. CHARACTERIZATION

High-resolution transmission electron microscopy (HR-TEM) was performed using a LEO 912 AB microscope with an electron beam accelerating voltage of 120 kV. Field emission scanning electron microscopy (FE-SEM) analysis was conducted on a TESCAN instrument. The UV-VIS absorption spectra of the samples were recorded in the 300-700 nm range using a Varian spectrophotometer. X-ray diffraction (XRD) analysis was carried out with a Shimadzu XRD-6000 powder diffractometer using CuKα radiation, with a diffraction angle range between 20° and 80°. Fourier transform infrared (FT-IR) spectra were obtained using a Thermo Nicolet FT-IR spectrometer. The crystallite size was determined using the Debye-Scherrer formula.

IV. DISCUSSION OF ANALYSIS

A. XRD Analysis

At room temperature, X-ray diffraction (XRD) tests were conducted to examine the phase purity and lattice structure of the as-obtained photocatalysts. The diffraction patterns of In_2O_3, N,S-rGO, and In_2O_3/N,S-rGO nanocomposites are shown in Figure 1, following two hours of sintering at 500 °C. Diffraction peaks observed at 21.4°, 30.5°, 35.4°, 50.9°, and 60.5° correspond to the (211), (222), (400), (440), and (622) planes of the In_2O_3 nanorods, which match the JCPDS reference no. 06416. The nanorods had a lattice parameter of a = 10.118 Å.

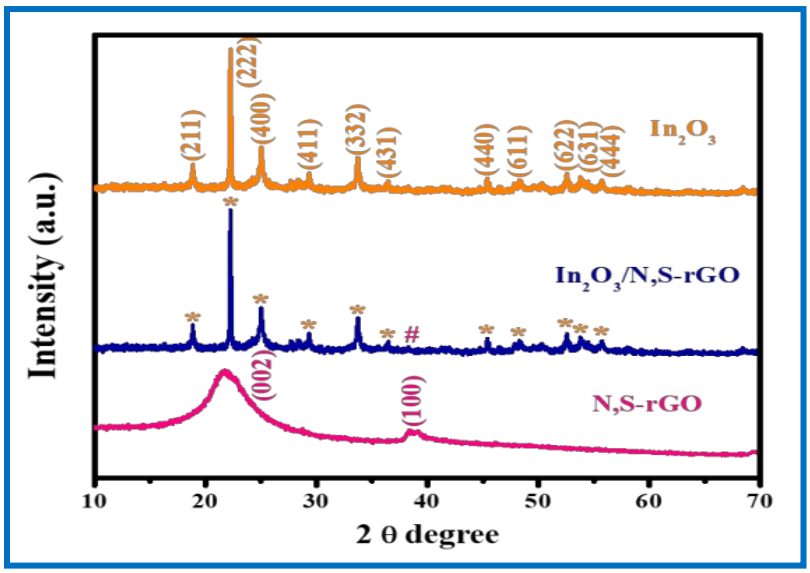

Fig. 1 XRD spectra for In_2O_3, N,S-rGO, and In_2O_3/N,S-rGO nanocomposite

Based on the available data, the XRD pattern produced can be indexed to the body-centered cubic structure of In_2O_3 [6]. Due to the low nitrogen concentration and weak S-rGO diffraction intensity, no peaks were observed for N,S-rGO and In_2O_3/N,S-rGO. This could be explained by the relatively low concentration of the composite and the weak intensity of rGO [25].

B. FT-IR Analysis

The characteristic peaks corresponding to the In-O asymmetric stretching vibrations were detected at 605, 563, and 430 cm^{-1}. On the surface of In_2O_3, the solid adsorption peaks at 3481 and 1630 cm^{-1} indicate the stretching vibration and in-plane deformation vibration of the O-H bond, respectively [26]. The C-N and C-S vibrations are represented by strong bands at 1172-1189 cm^{-1} and 1522-1573 cm^{-1}, respectively [27]. The wavelength corresponding to the C=N vibration suggests that GO has C double bonds with N dopants from thiourea, while the C-N and/or C-S vibrations indicate that GO has C single bonds with N and/or S dopants from thiourea. The stretching vibration of In-O-In bonds is represented by the broad infrared band at low frequency in the In_2O_3/N,S-rGO nanocomposite, and the bond at 556 cm^{-1} is due to the In-O vibration [28]. Additionally, a new absorption band at 1642

cm^{-1} was detected, which may be related to the skeletal vibration of the rGO sheets. The C=O and C-OH vibrations at 1719 and 1048 cm^{-1}, respectively, are represented by peaks in the In_2O_3/N,S-rGO composite, but they are not visible [29]. According to these results, the oxygen functional groups of N,S-rGO were removed, and its size decreased during the annealing of the In_2O_3/N,S-rGO composite [30].

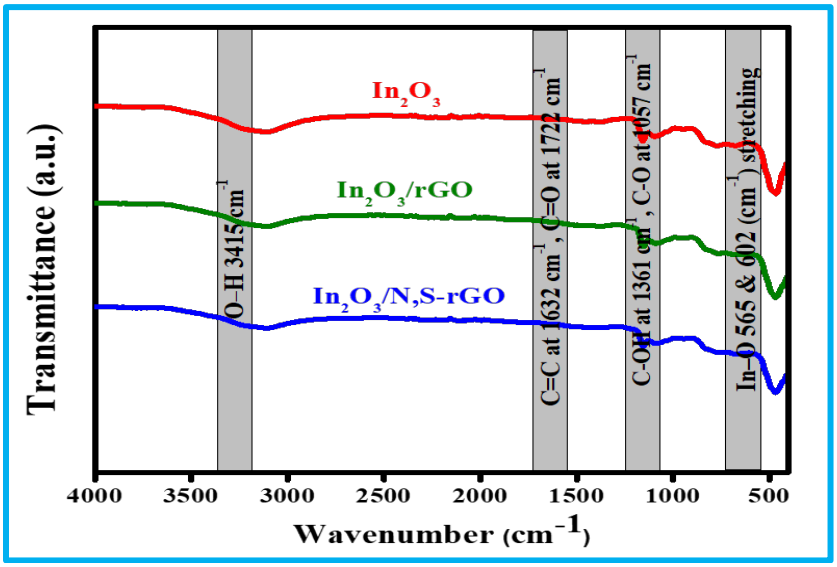

Fig. 2 FT-IR spectra for In_2O_3, N,S-rGO, and In_2O_3/N,S-rGO

C. FE-SEM and HR-TEM Images

Our SEM and TEM analyses of the produced nanocomposites allowed us to characterize additional morphologies and particle sizes. Figure 3 shows the SEM and TEM images of In_2O_3, N,S-rGO, and In_2O_3/N,S-rGO composites obtained with secondary electrons. The micrographs in Figures 3(b) and (e) show the morphology of pure In_2O_3, which is described as a rod-like structure, and thus they are referred to as nanorods. These nanorods often have a homogeneous, monodispersed structure.

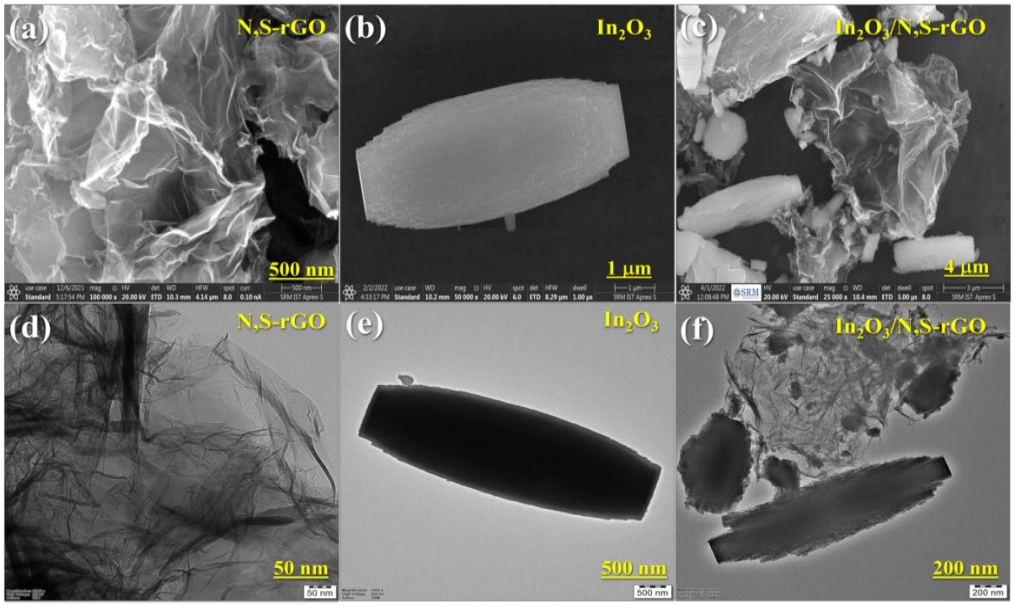

Fig. 3 FE-SEM and HR-TEM images of (a) N,S-rGO, (b) In_2O_3 (c) In_2O_3/N,S-rGO

As observed in Figures 3(a) and (d), the N,S-rGO images display thin, transparent sheets with creases and folds. The correlated skeleton and highly porous network structure of this overlapping network is evident. During the hydrothermal process, N and S atoms replace sp^2 C atoms and oxygen functional groups on the GO surface, resulting in structural defects that likely cause the wrinkle appearance and overlapping formation. Furthermore, the external carbon layer prevents aggregation and enhances the stability of the nanoparticles. The composite In_2O_3/N,S-rGO

contains a nanorod-layered structure, as demonstrated by the micrographs in Figures 3(c) and (f). The composite's micrograph shows many In_2O_3 nanorods deposited on the surface of the N,S-rGO nanosheet. This confirms the effective creation of a hybrid heterostructure combining layered N,S-rGO nanosheets with rod-like In_2O_3. These micrographs provide additional confirmation that adding In_2O_3 to N,S-rGO did not alter the material's initial rod-like shape. According to the images in Figures 3(b) and (c), the nanorods' average lengths range from 200 to 500 nm, and their particle sizes range from 1 to 4 µm. All of the findings point to the successful preparation of the In_2O_3/N,S-rGO composite, which is consistent with other research. According to [31], N and S dual doping may increase the chemical activity and electronic transport efficiency of the carbon layer, potentially enhancing the carriers' ability to separate during photocatalytic processes.

D. UV-Visible Diffuse Analysis

The UV-Vis diffuse reflectance profiles of the produced photocatalyst samples were determined by measuring their photoresponse, as shown in Figure 4.

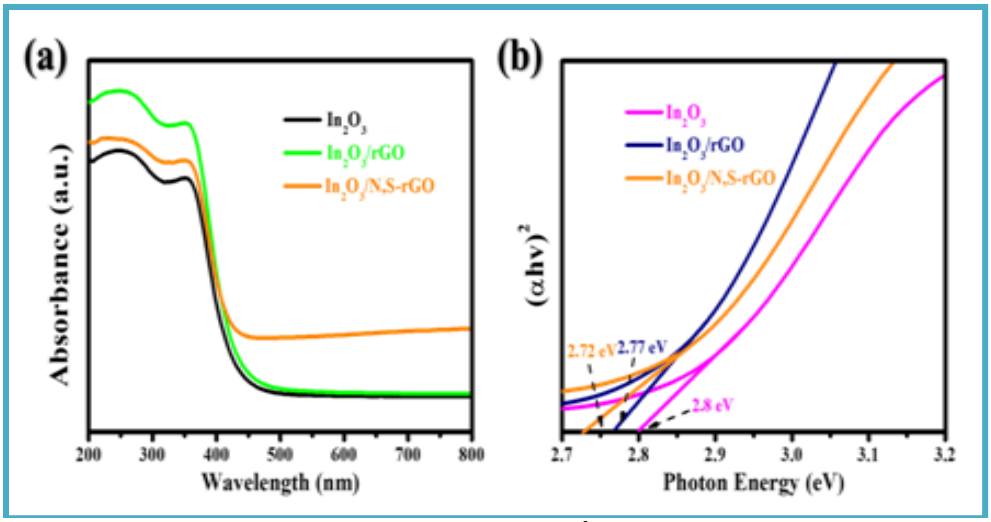

Fig. 4 (a) UV−Vis Diffuse reflectance spectra and (b) Tauc plots of $(\alpha h\upsilon)^2$ vs photon energy (eV) of the In_2O_3, In_2O_3/rGO and In_2O_3/N,S-rGO nanocomposites

The photoabsorptive capacity of a photocatalyst is known to affect its photocatalytic activity as well as other applications [32]. In the visible range, all of the generated photocatalysts exhibited a notable absorption response, as shown in Figure 4(a). At 460 nm, the optical absorption edges of each sample were observed. Tauc plots ($(\alpha h\nu)^2$ vs. the photon energy ($h\nu$)) were used to determine the bandgap energy levels of the as-prepared photocatalysts, where α, h, and ν represent the absorption coefficient, Planck's constant, and light frequency, respectively. Optical performance can be enhanced by combining light-absorbing materials and noble metals with a composite photocatalyst [33]. As shown in Figure 4(b), the direct bandgaps of In_2O_3, N,S-rGO, and In_2O_3/N,S-rGO were determined to be 2.8, 2.77, and 2.72 eV, respectively, based on the intercepts of the extrapolated linear fits of the Tauc plots.

V. CONCLUSION

In conclusion, In_2O_3 nanorods were prepared by the hydrothermal method and decorated with N,S-rGO using a simple in-situ co-precipitation technique. According to the results of the various characterization techniques, the ternary hybrid sample (In_2O_3/N,S-rGO) exhibits a cooperative morphology and a smaller bandgap that shifts to the visible light absorption region. Large-sized, regular-morphology N,S-codoped rGO-coated In_2O_3 nanoparticle semiconductor photocatalysts show synergistic effects, such as enhanced photocatalytic activity, decreased surface area and reactive sites, and excellent mobility and efficiency of photogenerated charge carriers. The synthesis method is simple, addressing the challenge of recycling. From the characterization results, we infer that our In_2O_3/N,S-rGO nanocomposite is a feasible semiconductor photocatalyst that is inexpensive, easy to assemble, and environmentally benign.

ACKNOWLEDGMENT

TETFUND provided financial support for this study through the administration of the Federal Polytechnic Kaura Namoda, located in Zamfara State, Nigeria.

REFERENCES

[1] R. Sorna Prema, S. Kandasamy, and K. Thirugnanasambandham, "Treatment of sea food industry wastewater using zinc oxide nano catalyst based photo oxidation process," *Asian Journal of Science and Applied Technology*, vol. 6, no. 2, pp. 22-27, 2017.

[2] S. Mohan, B. M. Nagabhushana, Chikkahanumantharayappa, and C. Shivakumara, "Removal of an azo dye Congo Red from aqueous solution by electro coagulation associated with the in-situ adsorption process," *Asian Journal of Science and Applied Technology*, vol. 10, no. 1, pp. 5-12, 2021.

[3] P. Muthuraman, M. Rajamani, and A. Xavier, "Amputate of assorted dyes from polluted aqueous solution using novel low cost adsorbents," *Asian Journal of Science and Applied Technology*, vol. 6, no. 2, pp. 14-21, 2017.

[4] S. Dutta, B. Gupta, S. K. Srivastava, and K. G. Ashok, "Recent advances on the removal of dyes from wastewater using various adsorbents: A critical review," *Mater. Adv.*, vol. 2, pp. 4497-4531, 2021.

[5] K. Zhang, M. Zhou, C. Yu, K. Yang, X. Li, W. Dai, J. Guan, Q. Shu, and W. Huang, "Construction of S-scheme g-C3N4/ZrO2 heterostructures for enhancing photocatalytic disposals of pollutants and electrocatalytic hydrogen evolution," *Dye. Pigment.*, vol. 180, p. 108525, 2020.

[6] V. Hasija, P. Raizada, V. Thakur, A. P. Aslam, M. A. Abdullah, and P. Singh, "An overview of strategies for enhancement in photocatalytic oxidative ability of MoS2 for water purification," *J. Environ. Chem. Eng.*, vol. 8, no. 5, p. 104307, 2020.

[7] L. Dai, X. L. Chen, J. K. Jian, M. He, T. Zhou, and B. Q. Hu, "Fabrication and characterization of In2O3 nanowires," *Appl. Phys. A Mater. Sci. Process.*, vol. 75, pp. 687-689, 2002.

[8] H. Dong, M. Xiao, S. Yu, H. Wu, Y. Wang, J. Sun, G. Chen, and C. Li, "Insight into the activity and stability of RhxP nano-species supported on g-C3N4 for photocatalytic H2 production," *ACS Catal.*, vol. 10, no. 1, pp. 458-462, 2020.

[9] A. Kubacka, M. S. Diez, D. Rojo, R. Bargiela, S. Ciordia, I. Zapico, J. P. Albar, C. Barbas, V. A. P. Martins dos Santos, and M. Fernández-García, "Understanding the antimicrobial mechanism of TiO2-based nanocomposite films in a pathogenic bacterium," *Sci. Rep.*, vol. 4, pp. 1-9, 2014.

[10] S. Banerjee, D. D. Dionysioub, and S. C. Pillai, "Self-cleaning applications of TiO2 by photo-induced hydrophilicity and photocatalysis," *Appl. Catal. B*, vol. 176-177, pp. 396-428, 2015.

[11] S. Liming, L. Rong, Z. Wenwen, Y. Yusheng, W. Xiaojun, H. Xiguang, and Y. Zhao, "Double-shelled hollow rods assembled from nitrogen/sulfur-codoped carbon coated indium oxide nanoparticles as excellent photocatalysts," *Nature Commun.*, vol. 10, no. 1, pp. 1-10, 2019, doi: 41467-019-10302-0.

[12] L. Wang, J. Zhao, H. Liu, and J. Huang, "Design, modification, and application of semiconductor photocatalysts," *J. Colloid Interface Sci.*, vol. 420, pp. 10-20, 2019.

[13] A. Qurashi, E. M. El-Maghraby, T. Yamazaki, Y. Shen, T. Kikuta, "A generic approach for controlled synthesis of In2O3 nanostructures for gas sensing applications," *J. Alloys Compd.*, vol. 481, pp. L35-L39, 2009.

[14] N. U. Sangari and P. Velusamy, "Enhanced photodecolorisation of Acid Blue 9 dye by ZnO in presence of beta cyclodextrin in aqueous solution under UV light," *Asian Journal of Science and Applied Technology*, vol. 8, no. 2, pp. 7-16, 2019.

[15] D. Chatterjee and A. Mahata, "Visible light induced photo-degradation of organic pollutants on dye adsorbed TiO2 surface," *J. Photochem. Photobiol. A Chem.*, vol. 153, pp. 199-204, 2002.

[16] H. Feng, Y. F. Wei, and S. L. He, "Controlled synthesis of flower-like In2O3 microrods and their highly improved selectivity toward ethanol," *Sensors Actuators B Chem.*, vol. 235, pp. 86-93, 2016.

[17] G. Tian, Y. Chen, K. Pan, D. Wang, W. Zhou, Z. Ren, and H. Fu, "Efficient visible light induced degradation of phenol on N-doped anatase TiO2 with large surface area and high crystallinity," *Appl. Surf. Sci.*, vol. 256, no. 12, pp. 3740-3745, 2010.

[18] F. Hui and C. Bu, "DFT description on electronic structure and optical absorption properties of anionic S-doped anatase TiO2," *J. Phys. Chem. B*, vol. 110, pp. 17866-17871, 2006.

[19] M. F. Smith, K. Setwong, R. Tongpool, D. Onkaw, S. Naphattalung, S. Limpijumnong, and R. Rujirawat, "Identification of bulk and surface sulfur impurities in TiO2 by synchrotron X-ray absorption near edge structure," *Appl. Phys. Lett.*, vol. 91, p. 142107, 2007.

[20] F. Wan, H. Y. Zhuo, X. G. Han, W. M. Chen, and D. Sun, "Foam-like CoO@N, S-codoped carbon composites derived from a well-designed N,S-rich Co-MOF for lithium-ion batteries," *J. Mater. Chem. A*, vol. 5, pp. 22964-22969, 2017.

[21] F. Gao, J. Yuan, X. Huang, R. Lei, C. Jiang, J. Zhuang, and P. Liu, "Directional transfer of photo-generated charges mediated by cascaded dual defects in ternary photocatalyst ZnS/ZnO-In2O3 with enhanced photocatalytic performance," *J. Colloid Interface Sci.*, vol. 602, pp. 261-273, 2021.

[22] A. Uddin, A. Rauf, T. Wu, R. Khan, Y. Yu, L. Tan, F. Jiang, H. Chen, "In2O3/oxygen doped g-C3N4 towards photocatalytic BPA degradation: Balance of oxygen between metal oxides and doped g-C3N4," *J. Colloid Interface Sci.*, vol. 602, pp. 261-273, 2021.

[23] S. Wang, B. T. Guan, and X. W. D. Lou, "Construction of ZnIn2S4-In2O3 hierarchical tubular heterostructures for efficient CO2 photoreduction," *J. Am. Chem. Soc.*, vol. 140, no. 15, pp. 5037-5040, 2018.

[24] F. Kleitz, S. H. Choi, and R. Ryoo, "Cubic Ia3d large mesoporous silica: Synthesis and replication to platinum nanowires, carbon nanorods and carbon nanotubes," *Chem. Commun.*, vol. 17, pp. 2136-2137, 2003.

[25] L. C. Chen, Y. J. Tu, and Y. S. Wang, "Characterization and photoreactivity of N-, S-, and C-doped ZnO under UV and visible light illumination," *J. Photochem. Photobiol. A Chem.*, vol. 199, no. 2-3, pp. 170-178, 2008.

[26] X. Li, Y. Feng, M. Li, W. Li, H. Wei, and D. Song, "Smart hybrids of Zn2GeO4 nanoparticles and ultrathin g-C3N4 layers: Synergistic lithium storage and excellent electrochemical performance," *Adv. Funct. Mater.*, vol. 25, no. 44, pp. 6858-6866, 2015.

[27] M. Zarei, "Ultrasonic-assisted preparation of ZrO2/g-C3N4 nanocomposites with high visible-light photocatalytic activity for degradation of 4-chlorophenol in water," *Water-Energy Nexus*, vol. 3, pp. 135-142, 2020.

[28] Y. Song, Y. Ding, F. Wang, Y. Chen, and Y. Jiang, "Construction of nano-composites by enzyme entrapped in mesoporous dendritic silica particles for efficient biocatalytic degradation of antibiotics in wastewater," *Chem. Eng. J.*, vol. 375, p. 121968, 2019.

[29] T. He, Y. Wu, C. Jiang, Z. Chen, Y. Wang, G. Liu, X. Zhenggang, N. Ge, C. Xiaoyong, and Z. Yunlin, "Novel magnetic Fe3O4/g-C3N4/MoO3 nanocomposites with highly enhanced photocatalytic activities: Visible-light-driven degradation of Tetracycline from aqueous environment," *PLoS ONE*, vol. 15, no. 8, p. e0237389, 2020.

[30] P. Ding, H. Ji, P. Li, Q. Liu, Y. Wu, M. Guo, Z. Zhou, S. Gao, W. Xu, W. Liu, Q. Wang, and S. Chen, "Visible-light degradation of antibiotics catalyzed by titania/zirconia/graphitic carbon nitride ternary nanocomposites: A combined experimental and theoretical study," *Appl. Catal. B Environ.*, vol. 300, p. 120633, 2021.

[31] Q. Wang, Y. Chen, X. Liu, L. Li, L. Du, and G. Tian, "Sulfur doped In2O3-CeO2 hollow hexagonal prisms with carbon coating for efficient photocatalytic CO2 reduction," *Chem. Eng. J.*, vol. 421, p. 129968, 2021.

[32] Q. Wang, Y. Chen, X. Liu, L. Li, L. Du, and G. Tian, "Sulfur doped In2O3-CeO2 hollow hexagonal prisms with carbon coating for efficient photocatalytic CO2 reduction," *Chem. Eng. J.*, vol. 421, p. 129968, 2021.

[33] A. Manickavasagan, G. Kadarkarai, K. Murugesan, S. Karunamoorthy, L. P. Seenivasan, M. Velluchamy, and A. Jang, "Reduction of hexavalent chromium and degradation of tetracycline using a novel indium-doped Mn2O3 nanorod photocatalyst," *J. Hazard. Mater.*, vol. 397, p. 122885, 2020.